Science of the Total Environment 903 (2023) 166118

Contents lists available at ScienceDirect

Science of the Total Environment

journal homepage: www.elsevier.com/locate/scitotenv

Improving food security and farmland carbon sequestration in China through enhanced rock weathering: Field evidence and potential assessment in different humid regions

Fuxing Guo [a,b], Haowei Sun [a,c], Jing Yang [a], Linsen Zhang [d], Yan Mu [e], Yanping Wang [a,b,f], Fuyong Wu [a,b,*]

[a] College of Natural Resources and Environment, Northwest A&F University, Yangling 712100, Shaanxi, PR China
[b] Key Laboratory of Plant Nutrition and the Agri-environment in Northwest China, Ministry of Agriculture, Yangling 712100, Shaanxi, PR China
[c] State Key Laboratory of Soil Erosion and Dryland Farming on the Loess Plateau, Institute of Soil and Water Conservation, Chinese Academy of Sciences & Ministry of Water Resources, Yangling 712100, China
[d] College of Horticulture, Northwest A&F University, Yangling 712100, Shaanxi, China
[e] College of Landscape Architecture and Arts, Northwest A&F University, Yangling 712100, Shaanxi, China
[f] Fuping Modern Agricultural Comprehensive Experimental Demonstration Station, Northwest A&F University, Fuping 711700, Shaanxi, China

HIGHLIGHTS

- The field influence of farmland ERW in different humid regions was explored
- Farmland ERW increased crop yield in the humid region by 13.5 ± 5.2 %
- Carbon sequestration of farmland ERW in China reached 0.28–0.40 Gt CO_2 yr^{-1}
- Precipitation and soil pH drive the field effect of ERW
- Contribution of management factors, especially fertilization, cannot be disregarded

GRAPHICAL ABSTRACT

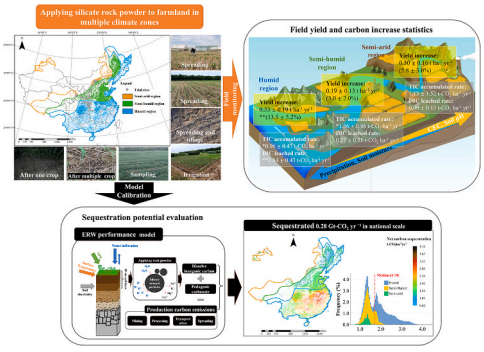

ARTICLE INFO

Editor: Jay Gan

Keywords:
Climate change
Enhanced basalt weathering
Soil inorganic carbon
Crop productivity
Soil acidification

ABSTRACT

Enhanced rock weathering (ERW) in farmland is an emerging carbon dioxide removal technology with crushed silicate rocks for soil improvement. However, due to climatic variability and field data limitations, uncertainties remain regarding the influence of ERW on food security and soil carbon pools in temperate regions. This study focused to evaluate the crop productivity and carbon sequestration potential of farmland ERW in China by conducting field monitoring in different humid regions and ERW performance model. Additionally, the contribution of climate, soil, and management factors to ERW-mediated yield and carbon sequestration changes was explored using random forest and correlation networks. Field monitoring indicated that farmland ERW significantly improved crop yield in humid region (13.5 ± 5.2 %), along with notable improvements in soil pH and available nutrients. Precipitation (10.4–16.7 %) and soil pH (9.7–16.8 %) had the highest contribution on ERW

* Corresponding author.
E-mail address: wfy09@163.com (F. Wu).

https://doi.org/10.1016/j.scitotenv.2023.166118
Received 2 June 2023; Received in revised form 2 August 2023; Accepted 5 August 2023
Available online 11 August 2023

mediated yield and carbon sequestration changes, but the contribution of management factors (24–26.2 %), especially N input (2.7–7.0 %), should not be disregarded. The model evaluation demonstrated that the carbon sequestration rate of farmland ERW in China can reach 0.28–0.40 Gt yr^{-1}, thereby presenting an opportunity to expand and accelerate the nationally determined contributions of China. The mean sequestration cost of farmland ERW was 633 ± 161 CNY ¥ t-CO_2^{-1}, which was an attractive sequestration price considering the positive benefits of rock powder on soil pH and nutrients. Deploying ERW in acidified and mineral nutrient deficient regions was able to serve as an alternative to lime and part chemical fertilizers to improve yield and maximize agricultural sustainability and resource co-benefits. Farmland ERW also has the potential to resource silicate waste to assist traditional, difficult-to-decarbonize industries to reduce carbon emissions. As a result, a comprehensive assessment of existing artificial silicate waste materials could further expand the application of farmland ERW.

1. Introduction

Considering the dependence of various sectors on carbon emissions and the urgent international emission reduction targets, negative emission technology (NET) becomes a more prominent role in future climate stability strategies (Rogelj et al., 2016; Amann and Hartmann, 2019; Nugroho et al., 2023). As the world's largest land user (Solinas et al., 2021), NETs based on agriculture had considerable potential on a global scale. For example, soil organic carbon sequestration could contribute around 5 Gt yr^{-1}, while bioenergy with carbon capture and storage, as well as biochar, could contribute 0.5–5.0 Gt yr^{-1} and 0.5–2 Gt yr^{-1} (Fuss et al., 2018; Renforth, 2019; Rinder and Hagke, 2021). However, studies have traditionally tended to focus only on the soil organic carbon sequestration pathways, while research about improving inorganic carbon was relatively lacking. Soil inorganic carbon (SIC) played a vital role in providing ecological service by balancing soil pH, improving nutrients and organic carbon (Wang et al., 2015; Raza et al., 2020). The loss of SIC was an essential sign of soil acidification and reduced fertility (Dang et al., 2022; Tao et al., 2022). Several studies have emphasized the rapid loss of SIC in agricultural soil, but this hidden danger is currently remaining under-appreciated (Zamanian et al., 2018; Song et al., 2022). Therefore, seeking a means to mitigate SIC losses has positive implications for food security and climate change.

The recent proposal of enhanced rock weathering (ERW) strategies has provided new ways for promoting inorganic carbon in farmland soils (Köhler et al., 2010; Hartmann et al., 2013; Beerling et al., 2020). Farmland ERW refers to the application of artificially crushed silicate rocks or materials on farmland to improve crop productivity and SIC (Renforth, 2012; Hartmann et al., 2013; Beerling et al., 2020). Silicate rock powder had the function of slow-release fertilizer, providing a variety of essential mineral nutrients (e.g., K, Ca, Mg, Fe, Mn) to the crop over a long period (Beerling et al., 2018). These mid- and micronutrients were often overlooked in the conventional commonly applied NPK fertilization programs (Swoboda et al., 2021). The addition of silicate also could correct soil acidity, reduce aluminum toxicity, and supply available silicon (Dietzen et al., 2018; Jariwala et al., 2022). Moreover, the theoretical carbon sequestration efficiency of ERW was substantial (Renforth, 2012; Moosdorf et al., 2014). Taking anorthite as an example (Eq. (1)), the weathering of primary silicate minerals produced secondary minerals (kaolinite), alkaline cations (Ca^{2+}), and promoted the conversion of atmospheric CO_2 to dissolved inorganic carbon (DIC) in the form of bicarbonate (HCO_3^-) (Penman et al., 2020; Cipolla et al., 2021; Rinder and Hagke, 2021).

$$CaAl_2Si_2O_8 + 2CO_2 + 3H_2O \rightarrow Al_2Si_2O_5(OH)_4 + 2HCO_3^- + Ca^{2+} \quad (1)$$

Ca^{2+} and DIC increased the carbonate saturation state, thereby promoted calcium carbonate as well as its subsequent preservation and burial in sediments (Eq. (2)):

$$Ca^{2+} + 2HCO_3^- \rightarrow CaCO_3 + CO_2 + H_2O \quad (2)$$

It is evident that silicate rocks can fix at least one mole of carbon dioxide for every two moles of positive charge released. Silicate rocks were distributed widely and contained a variety of mineral nutrients, so large-scale ERW on farmland was viable and essential to solving food security and climate change (Deer et al., 2013; Fuss et al., 2018). However, the current research was mainly focused on tropical regions, where the rock type was mainly ultrabasic rocks with rapidly weathered (such as dunite and wollastonite). While the research was relatively lacking with more commonly slowly-weathered silicate rock under different climatic conditions.

Ultrabasic rocks were relatively expensive and scarcely. Consequently, farmland ERW strategies based on such rocks were inevitably limited by costs and resources, even if they had a faster weathering rate and higher calcium and magnesium content. Moreover, ultrabasic rocks may be contained high levels of Ni and Cr elements, which may lead to the enrichment of heavy metal elements in crops (ten Berge et al., 2012; Amann et al., 2020; Kelland et al., 2020). Basalt was an ideal material for farmland ERW due to its wide distribution and including various nutrients as well as lower Cr and Ni (Beerling et al., 2018; Dalmora et al., 2020; Rinder and Hagke, 2021). Evaluative research based on the integrated performance models revealed that ERW with basalt at the farmland scale could potentially remove 0.5–2 Gt-CO_2 yr^{-1} globally (Beerling et al., 2020). However, field evidence of farmland ERW was infrequent. Although exogenous silicate rock powder was able to improve crop growth in strongly weathered soils of the tropics (Haque et al., 2019; Swoboda et al., 2021), the effect on larger areas of neutral or calcareous soils remained unclear. Stripping the soil conditions of strong acidity and high water flux, the nutrient benefits and carbon sequestration potential of the basalt may be limited. Therefore, a comprehensive field monitoring analysis encompassing different climate regions is necessary to further promote ERW technology at a larger scale.

China, as a major carbon-emitting country, is in a critical situation to achieve nationally determined contributions (NDCs) (Fu et al., 2015; Xiao et al., 2020; Zuo et al., 2023). The implementation of farmland ERW can contribute to fulfilling NDCs and alleviating the pressure of emission reduction policies (Beerling et al., 2020). We thus conducted a set of field monitoring experiments across semi-arid, semi-humid, and humid regions in China to evaluate the crop productivity and carbon sequestration of farmland ERW. We hypothesized that while the field performance of ERW may be somewhat dependent on precipitation and soil pH, basalt could still improve crop yield and SIC in a wider range of Chinese farmlands. The specific objectives of this study included: (1) exploring the response of crop growth, soil biogeochemistry, and inorganic carbon storage to ERW, (2) analyzing the environmental factors of yield and inorganic carbon change mediated by ERW, and (3) evaluating carbon sequestration and cost of farmland ERW in China based on an ERW performance model.

2. Materials and methods

2.1. Field experiment

2.1.1. Distribution of field experiment sites

The distribution of field experimental sites involved three climate zones in China: semi-arid, semi-humid, and humid regions (Fig. 1). The

basis for the regional division was the dry and wet conditions (precipitation 200–400, 400–800, and > 800 mm). The field experimental sites in the humid region were arranged in April 2019, with 12 sample sites, mainly concentrated at the junction of Shaanxi Province, Hubei Province, and Chongqing municipality. The field experimental sites in the semi-humid region were also deployed in 2019, distributed mainly in the Loess Plateau of northern Shaanxi and the Guanzhong Plain, with a total of 11 sites. The experimental sites in the semi-arid region were laid out in April 2021, concentrated around Liangcheng County in Inner Mongolia Autonomous Region and Yongjing County in Gansu Province, with the number of sites being 8. The climate and soil properties of field sites in each region is shown in *Fig. S1* and *Fig. S2*.

2.1.2. Source and characteristics of mixed silicate rock powder

A mixed silicate rock powder was made through five different sources of basalt gravel. The sources were Liangcheng of Inner Mongolia Autonomous Region (112.191°E, 40.509°N), Pingding of Shanxi Province (112.042°E, 37.037°N), Neixiang of Henan Province (111.688°E, 33.067°N), Jingshan of Hubei Province (113.209°E, 31.196°N) and Yongjing of Gansu Province (103.512°E, 36.022°N), respectively. To improve the nutrient supply and sequestration potential, we further added one plauenite, two phosphorus-bearing silicates (andesite and diabase), and two ultramafic rocks (peridotite and serpentine). Rocks were uniformly crushed twice (jaw and cone crusher), milled once (high energy ball milling), and passed through a 200-mesh sieve. Each rock powder was mixed in equal mass proportions and used for farmland.

Rock particle size was measured with the laser particle sizer (Mastersizer 2000, Malvern) (Arriaga et al., 2006), and the Brunauer-Emmett-Teller (BET) specific surface area was measured based on the BET N_2-adsorption method (Brunauer et al., 1938) with the specific surface area and pore size distribution analyzer (V-sorbx2800p, Gold APP). The average P80 (rock mass ratio with particle size less than this value reached 80 %) of the mixed rock powder was 38.4 ± 4.5 μm, and the mean BET specific surface area was 13.8 ± 2.7 $m^2\ g^{-1}$. The main element composition of the rock was analyzed by X-ray fluorescence (XRF, SPECTRO, MIDEX) and melting method (Amann et al., 2020; Haque et al., 2020). The trace element (Cd, Hg, As, and Pb) was analyzed by microwave digestion and the inductively coupled plasma optical emission spectrometer (ICP-OES; ARCOS, SPECTRO) (SAMR and SAC, 2020). The inorganic carbon content in rocks was measured using the combination method automatic carbon and nitrogen analyzer (Primacs SNC100, Skalar) to remove the influence of carbonate minerals. Rock powder mineral composition was measured by an X-ray diffractometer (XRD, D8 ADVANCE A25, Bruker) (Chung, 1974), Jade. 9 and standard card library PDF-4 + 2009 was adopted to analyze crystalline mineral phases. The chemical composition of basalt glass (*Table S1*) was determined based on the electron probe microanalyzers (JXA-8100, JEOL) (Sun et al., 2011). The minerals and elemental composition are shown in Table 1, and the specific analysis and XRD curve of each rock was referred to Guo et al. (2023).

2.1.3. Experimental design and sampling

At each field experiment site, three 5 m × 5 m monitoring quadrats were set for ERW treatment (T_{ERW}) with 10 kg m^{-2} (100 t ha^{-1}) mixed rock powder. Mixed rock powder was manually spread and incorporated into the 0–20 cm soil layer by tillage. The control treatments (T_C) were randomly placed in untreated areas of the same field and the replicates were three. Except for the mixed rock powder, other mineral-type soil amendments (such as lime) were avoided in all treatments.

Plant samples were collected in November and June each year. Based on the five-point sampling method (Gong, 2000; Ming, 2013), 1 m × 1 m sampling plots were set at the quadrat diagonal intersection and four corners located 1.0 m from the boundary, and all aboveground biomass in the five plots was collected (*Fig. S3*). This study involved four crops: corn, wheat, potatoes, and soybeans. Except for potato tubers, the plant samples were killed at 95 °C for 30 min and dried at 65 °C for 48 h to measure the dry weight. Potato yield referred to 20 % of the fresh weight of tubers, and other crop yield referred to the seed's dry weight.

The accumulation of soil inorganic carbon (TIC) in the surface layer (0–40 cm) and the DIC changes in 40–200 cm soil water samples leached from the surface layer were considered stable carbon sequestration items in this study. The reasons based on such depth were because (1) crop roots and nutrient supply were mainly distributed in 0–40 cm soil layers (Dong et al., 2016; Gai et al., 2018; Hao et al., 2018; Zhao et al., 2020), (2) the change of soil inorganic carbon (TIC) was relative sensitive in 0–40 cm soil layers (Li et al., 2007; Qiu et al., 2016; Han et al., 2018; Tao et al., 2022), (3) the infiltration depth of annual rainfall was between 80 and 180 cm in the study region (Li, 1983). Soil samples of 0–40 cm soil layer were taken in November every year from the center of each 1 × 1 sampling plot with a soil drill (10 cm increments). The soil water sample was collected in November 2022 using the clay tubes negative pressure collector. Clay tube heads (6 cm in length and 2 cm in diameter) were buried into the depth of 50, 70, 100, 140, and 180 cm at the soil sampling plot by a vacuum pump.

2.1.4. Analysis of soil and water samples

Sample analyses were conducted in the Key Laboratory of Plant Nutrition and the Agri-environment of the Ministry of Agriculture in Northwest China. To obtain direct and reliable field evidence, TIC in soil samples and DIC in soil water samples were directly measured by the TOC analyzer (TOC-L03030135, Shimadzu). Soil exchange nutrients (P, K, Ca, Mg, and Si) and cation in water samples (Ca, Mg, and Si) were measured using ICP-OES. For acid and neutral soils (inorganic carbon <1.2 g kg^{-1}), samples were extracted with 1 mol L^{-1} ammonium acetate solution (pH = 7) (MoA, 2006). For calcareous soils (inorganic carbon ≥1.2 g kg^{-1}), samples were extracted by 0.1 mol L^{-1}ammonium chloride (pH = 8.5)-ethanol solution (70 %) (MoA, 2008). Soil exchangeable P was extracted with 0.5 mol $L^{-1}NaHCO_3$. Soil pH was measured by FE28 pH Meter (Bao, 2000). In all analyses, each soil sample was repeated three times, and the maximum relative error (MRE) and relative standard deviation (RSD) were both <5.0 %.

The cumulative value of the layer-by-layer change was adopted to assess the effect of ERW. For example, the TIC sequestration caused by ERW was calculated by Eq. (3):

$$\Delta TIC = \left(\sum_{i=1}^{n} \left[d_i \times TIC_i^{TERW-TC} \times BD_i \right) \times \frac{M_{CO_2}}{M_C} - [\%CO_2 \times R_{Mix}] \right. \quad (3)$$

where, ΔTIC is the soil inorganic carbon sequestration caused by ERW (t-CO_2 ha^{-1} yr^{-1}); d_i is the depth of soil layer i (m); $TIC_i^{TERW-TC}$ is the TIC difference between T_C and T_{ERW} in soil layer i (g kg^{-1} yr^{-1}); BD_i is soil bulk density (g cm^{-3}); M_{CO2} and M_C is the molecular masses of CO_2 and C; $\%CO_2$ is the mass percentages of the CO_2 in the rock; R_{Mix} is the application rate of rock powder.

2.2. Environmental impact analysis

2.2.1. Collection of climate and management data

The data types and sources in this study are listed in *Table S2*. The climate impact factors dataset was collected from the National Meteorological Information Centre (NMIC, 2017), which included surface pressure, solar radiation, temperature, pre1cipitation, relative humidity, and wind speed. The evapotranspiration of each site was calculated based on the FAO-PM model (Allen et al., 1998). Farmland management factors were collected by surveying administrators and farmers, including slope, tillage method, planting pattern, fertilization, and irrigation.

2.2.2. Measurement of initial soil data

Soil impact factors measured included soil particle composition (sand and clay), moisture, pH, carbon component, cation exchangeable content (CEC), and available N, P, and K. The soil particle composition

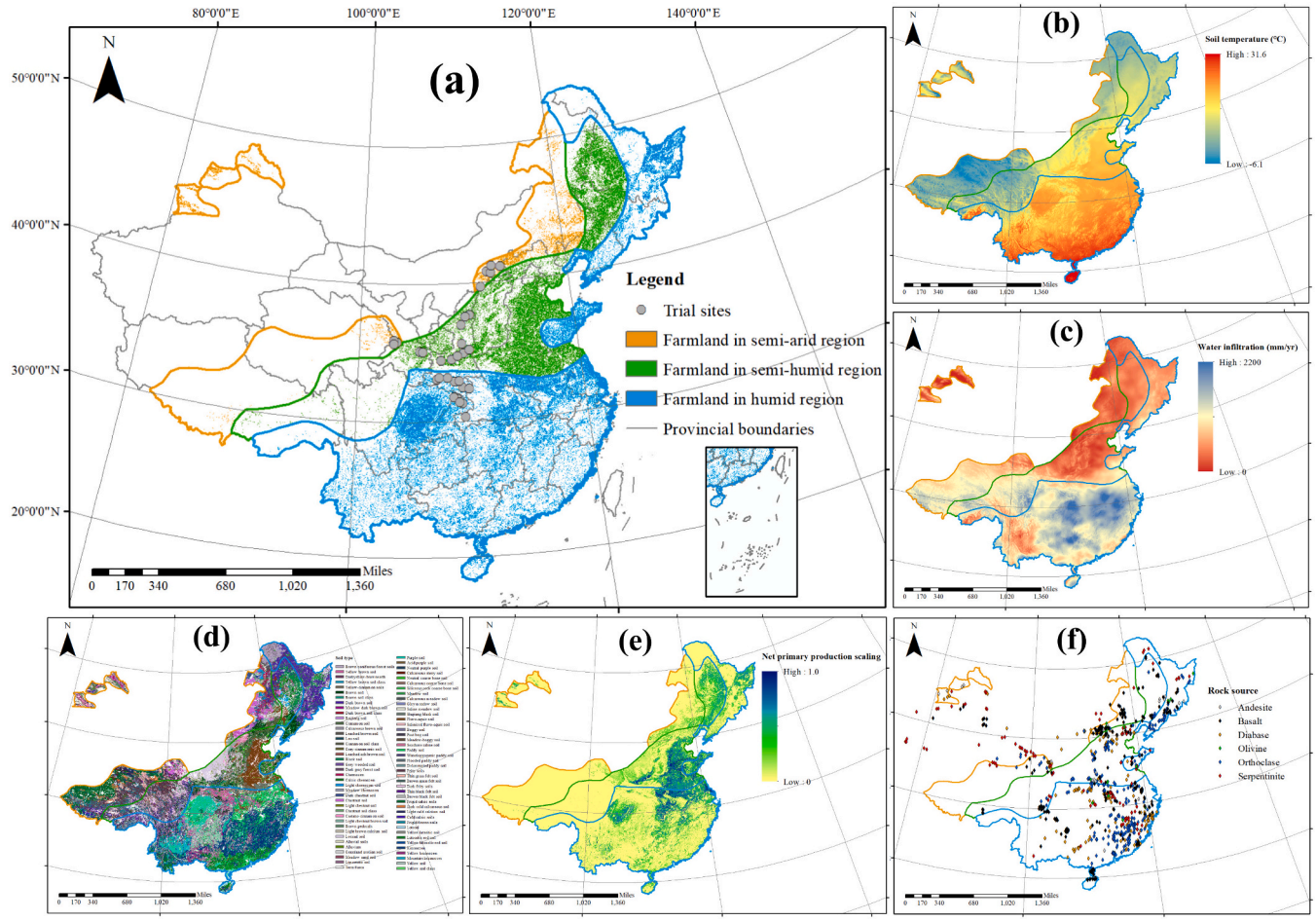

Fig. 1. Farmland area and the location of field experiments in different regions (a), and the spatial distribution of soil temperature (b), water infiltration (c), soil type (d), net primary production scaling (e), and rock source (f).

was measured using a laser particle sizer (Mastersizer 2000, Malvern) (Arriaga et al., 2006; Sochan et al., 2012). International classification standards were used to classify soil particles as sand (0.02–2 mm), and clay (<0.002 mm). Soil moisture was measured with the drying method, and soil available nitrogen was extracted using 1 mol L^{-1} KCl and measured using the AA3 continuous flow analyzer (AA3, SEAL) (Bao, 2000). The measurement of soil exchangeable cation and available P, K is referred to Section 2.1.3.

2.2.3. *Evaluating the contribution based on the random forest algorithm*

The feature importance of the random forest regression algorithm (Breiman, 2001; Elith et al., 2008; Li et al., 2021) was used to quantify the contribution of climate, soil, and management influence on yield, TIC, and DIC change. We optimized two hyperparameters of the RF model: the number of trees (n_estimators) and the random seed (random_state). Grid searching was utilized to find the optimal combination of hyperparameters (*Table S3*). The random forest was implemented

Table 1
Average mineralogy and elemental composition of mixed rock powder.

Mineral	Formula	Weight (%)	Oxide	Weight (%)	Trace element	Content (mg kg^{-1})
Plagioclase	$Ca_{0.68}Na_{0.32}Al_{1.68}Si_{2.32}O_8$	31.9 ± 20.3	SiO_2	49.7 ± 5.6	Cd	0.9 ± 0.6
Augite	$Ca_{0.78}Mg_{0.85}Na_{0.01}Mn_{0.01}Ti_{0.01}Al_{0.088}Fe_{0.32}Si_{1.94}O_6$	18.0 ± 11.2	Al_2O_3	13.4 ± 6.5	Hg	0.4 ± 0.4
Hornblende	$Ca_{1.8}Na_{0.5}Mg_{2.2}Fe_2Al_{2.4}Si_{6.4}O_{22.2}(OH)_{1.8}$	3.4 ± 4.5	Fe_2O_3	7.8 ± 4.0	As	5.2 ± 6.1
Montmorillonite	$Ca_{0.2}Al_2Mg_2Si_4O_{12.2}(OH)_2{\cdot}2H_2O$	1.4 ± 2.2	CaO	7.2 ± 4.3	Pb	50.5 ± 35.0
Chlorite	$Mg_{9.8}Fe_{0.6}Al_{3.28}Si_{6.32}O_{20.24}(OH)_{15.72}$	1.1 ± 2.1	MgO	10.6 ± 12.9	Cr	402.3 ± 223.8
K-Feldspar	$KAlSi_3O_8$	10.6 ± 23.9	K_2O	1.7 ± 3.1	Ni	248.6 ± 264.9
Forsterite	$Fe_{0.3}Mg_{1.7}SiO_4$	12.9 ± 23.5	Na_2O	2.2 ± 1.3	Sr	477.4 ± 296.9
Lizardite	$Mg_3Si_2O_5(OH)_4$	7.6 ± 22.7	P_2O_5	1.2 ± 1.4		
Apatite	$Ca_5(PO_4)_3(OH)$	2.6 ± 3.4	MnO	0.5 ± 0.4		
Ilmenite	$FeTiO_3$	1.9 ± 2.5	TiO_2	1.5 ± 1.6		
Basaltic-glass	$Na_{0.08}Ca_{0.1}Mg_{0.04}K_{0.1}Fe_{0.11}Al_{0.25}Si_{2.5}O_{5.74}$	6.4 ± 13.0	LOI	3.5 ± 1.1		
Quartz	SiO_2	1.5 ± 2.0	Total	99.3 ± 0.5		
Calcite	$CaCO_3$	0.8 ± 1.3	CO_2	0.6 ± 1.1		

Note: The mineral and elemental composition of mixed rock powder is the arithmetic average of ten rock powders, the specific analysis of each rock was mentioned in Guo et al. (2023).

using the scikit-learn (version 1.1.0) package in Python 3.8. The explained variance (R^2) and relative root mean square error (rRMSE) were used to evaluate model performance as follows:

$$R^2 = \frac{\sum_{i=1}^{n}(x(i)-\bar{x})(y(i)-\bar{y})}{\sqrt{\sum_{i=1}^{n}(x(i)-\bar{x})^2}\sqrt{\sum_{i=1}^{n}(y(i)-y)^2}} \quad (4)$$

$$RMSE = \sqrt{\frac{\sum_{i=1}^{n}(x(i)-y(i))^2}{\bar{n}}} \quad (5)$$

$$rRMSE = \frac{RMSE}{\bar{x}} \quad (6)$$

where $x(i)$ and $y(i)$ are the observed and predicted values, respectively; $\bar{x}$ and $\bar{y}$ denote the average observed and predicted values, respectively; and n is the number of samples.

2.2.4. Correlation network analysis of environmental impact factor

The correlation network analysis was adopted to visualize the co-linear relationships between the variables (Leroux et al., 2022). We calculated the direct correlations of climate, soil, and management drivers to yield, TIC, and DIC change, as well as the indirect correlations between climate and management drivers. Pearson correlation was used to calculate correlation coefficients between all paired variables, and only significant correlations were shown in the correlation network ($p < 0.05$).

2.3. Evaluating the ERW carbon sequestration potential in China farmland

2.3.1. Description of ERW performance model

The ERW performance model (Beerling et al., 2020) was used to evaluate the sequestration potential of farmland ERW strategies in three regions of China. The model was adopted is due to (1) the simplified single average particle diameter was replaced with the logarithmic normal particle distribution of rocks, (2) the fractal dimension of surface roughness was used to link the reaction surface with the change of basalt mass, (3) it was able to reflect various influencing factors including rock dissolution kinetics (*Table S4*), chemical affinity, soil hydrology, temperature, pH, and crop growth. The core of the model consists of a solute transport equation and a mass balance equation. The solute transport equation (Eq. (7)) was used to determine the dissolved concentration of mineral i (c_i mol L^{-1}):

$$\theta\frac{\partial c_i}{\partial t} = -Q\frac{\partial c_i}{\partial z} + R_i\left(1-\frac{c_i}{c_{eqi}}\right) \quad (7)$$

where θ is soil moisture ($m^3\ m^{-3}$), t is time (year), Q is vertical water flux (m yr^{-1}), z is vertical distance (m), R_i is the weathering rate of mineral i (mol L^{-1} yr^{-1}), and C_{eqi} is the solution concentration in equilibrium with mineral i.

The mass balance equation was used to monitor the exogenous minerals mass change, as Eq. (8):

$$\frac{\partial M_i}{\partial t} = -R_i\left(1-\frac{c_i}{c_{eqi}}\right) \quad (8)$$

where M_i is the exogenous minerals mass (mol L^{-1}).

An additional Ca ions transport equation (Eq. (9)) was employed to calculate secondary carbonate precipitation:

$$\frac{\partial Ca}{\partial t} = -Q\frac{\partial Ca_{sol}}{\partial z} + \sum_{i=1}^{n} R(M_i)M_{cai} \quad (9)$$

where Ca (mol L^{-1}) is the concentration of Ca ions retained in the soil, Ca_{sol} (mol L^{-1}) is the concentration of Ca ions in the soil solution, n is the number of minerals in rock powder, $R(M_i)$ is the weathering rate of mineral i at a mass change of M_i, and M_{cai} is the number of moles of Ca in mineral i. Ca_{sol} is the minimum value of both Ca and Ca_{sat}, and Ca ions in the secondary precipitation, Ca_{precip} (mol L^{-1}) = $Ca - Ca_{sol}$.

The total weathered mixed rock powder was the sum of dissolved minerals:

$$M_{total} = \sum_{i=1}^{n}\Phi\int_{z=0}^{L} C_i(t,z)dz + \int_{t=0}^{tf} C_i(t,L)dt \quad (10)$$

where L is the total depth, and tf is the total time.

Moreover, in cyclic modeling, under-weathered minerals will continue to weather in the next cycle with the newly added minerals.

$$M(t) = \int_0^{\infty} f_1(t\,r) + f_2(t\,r)\cdots\cdots dr \quad (11)$$

where $f_1(t\,r)$ is exogenous mineral mass and its particle size distribution in the first cycle, $f_2(t\,r)$ is exogenous mineral mass and its particle size distribution in the second cycle. The spatial dataset used for the model operation is listed in Fig. 1 and *Table S2*, and for a more detailed model description see Beerling et al. (2020).

2.3.2. Boundary condition, calibration and validation

The Dirichlet boundary condition in the soil surface was set as dissolved concentration c = 0 at soil depth z = 0, and the Neumann boundary condition at the bottom where the concentration gradient was zero. The applied mixed rock powder was evenly distributed in the 0–20 cm soil layer, and the concentration of minerals in the soil water solution is set to 0 at time $t = 0$.

The chemical affinity term of plagioclase was calibrated through the comparison of changes in dissolved products and secondary calcium carbonate between field monitoring and model simulation (*Fig. S4*), while the affinity term of other minerals was no longer considered because of low content proportion and long simulated weathering cycle. The relationship of P80, specific surface area, and grinding energy consumption was also recalibrated using rock data from this study (*Fig. S5*). Based on a compilation of mineral dissolution rates (Brantley et al., 2008), we validated the ERW performance model for basalt, olivine, and K-feldspar (*Fig. S6*).

2.3.3. Carbon sequestration statistics

The carbon sequestration caused by ERW was calculated through the accumulation of cations (Ca^{2+} Mg^{2+} Na^{+} and K^{+}) in the subsoil layer (leaching depth > 40 cm) and soil layer (0–40 cm). In the former, the capture of CO_2 was calculated through Eq. (12):

$$DIC = \left(2\left(C_{Ca^{2+}} + C_{Mg^{2+}}\right) + C_{K^{+}} + C_{Na^{+}}\right) \times \omega \times M_{CO_2} \quad (12)$$

where DIC is CO_2 sequestration in soil drainage (t ha^{-1} yr^{-1}), $C_{Ca^{2+}}$, $C_{Mg^{2+}}$, $C_{K^{+}}$ and $C_{Na^{+}}$ is the weathering cation flux in soil drainage (mol ha^{-1} yr^{-1}), ω is (0.85, referring to previous studies) is the additional cation flux loss through ocean carbonate chemistry (Renforth, 2012; Amann et al., 2020), M_{CO_2} is the the molecular mass of CO_2. In the carbonate precipitation, the accumulation of one mol Ca^{2+} corresponded to the capture of one mol of CO_2.

2.3.4. Determination of secondary emission and costs

The carbon emissions were generated in four processes: rock mining, processing, transportation, and application. Carbon emissions were the product of the amounts of rock powder applied and the emission factors. The energy consumption coefficient and emission factor are listed in *Table S5*. The energy consumption during the processing process was exponentially related to the logarithm of rock P80 in the ERW performance model (see *Fig. S5*). The transportation distance was simplified as the linear distance between each grid and the rock source (*Fig. S7*). Due

to considerations of mining restrictions and environmental policies in China, rock sources were only referred to the existing silicate quarry in China (NGA, 2019) (Fig. 1f). The total cost included the operating costs of quarries, electricity, and oil costs during the rock production process. A mining component cost assessment framework was localized through gross national income and diesel prices of China in 2019 (*Table S6*) (Beerling et al., 2020). The electricity price refers to the sales electricity price of each province's industrial (voltage level is 1–10 kV) average period (*Fig. S7*).

2.3.5. Baseline and different scenarios

The baseline was based on the field monitoring experiment in Section 2.1. The mixed rock powder was applied with 100 t ha^{-1} per 5 years and simulated continuously for 20 years to calculate the multi-year average sequestration rate (*Fig. S8*). The P80 of rock particle size was set to 38.5 μm. The electric energy emission factor adopted the emission factor of operation margin (EFOM, which reflected a pessimistic energy policy dominated by fossil fuels). The transportation method is heavy diesel trucks. On a baseline basis, different scenarios were established by adjusting application rate (50, 25 t ha^{-1} per 5 years), P80 (increased by 5 times, decreased by 5 times), electric energy emission factor of build margin (EFBM, optimistic emission factor calculated based on 20 % new power plants in China), and transportation mode.

2.4. Statistical analysis

The non-parametric Kruskal-Wallis test ($p < 0.05$) was used to analyze significance because this test requires no normally distributed data. This analysis was performed by utilizing the statsmodels (version 0.12.2) package in Python 3.8.

3. Results

3.1. Field experiment

3.1.1. Crop productivity response to enhanced rock weathering

The comparison results of yield and biomass (Fig. 2) indicated that T_{ERW} displayed considerable crop yield increases effects (13.5 ± 5.2 %) in the humid region, which contributed to offsetting the costs associated with mixed rock powder application. In the semi-arid region, ERW significantly ($p < 0.05$) increased the spring wheat yield (13.9 ± 5.6 %), but there was no significant difference in regional mean yield (*Fig. S9*). In humid region, the yield of corn, winter wheat, and soybeans all significantly increased ($p < 0.05$), and the mean yield and biomass of T_{ERW} increased by 0.53 ± 0.19 t ha^{-1} and 0.92 ± 0.21 t ha^{-1} (17.9 ± 5.6 %).

3.1.2. Soil and leachate biogeochemistry response to enhanced rock weathering

The improvement of soil pH and exchangeable nutrients (Table 2) may explain the differences in crop yield changes among different regions. T_{ERW} significantly increased ($p < 0.05$) soil pH only in humid region, with an increase of 0.17 ± 0.13 units yr^{-1}. This result supported the view that ERW can prevent soil acidification and replace lime in low soil pH regions (Dietzen et al., 2018; Kelland et al., 2020). The comparison of soil exchangeable nutrients revealed that T_{ERW} exhibited more considerable multiple nutrient effects in the humid region, but the significant influence in the semi-arid and semi-humid regions was only concentrated on Mg and Si. P, K, Ca, Mg, and Si were all significantly ($p < 0.05$) increased in humid region. The increment of P and K in the humid region was equivalent to 10 and 19 % of the average annual fertilizer input. Chemical analysis of the leachate showed that T_{ERW} significantly ($p < 0.05$) increased the leachate pH in the semi-humid and humid region by 0.13 and 0.24 units yr^{-1}, respectively. Soluble element analysis showed that Ca and Mg showed significant changes ($p < 0.05$) in the semi-humid and humid regions. The element of Si was without significant changes in the leachate of the three regions.

3.1.3. The effect of enhanced rock weathering on carbon sequestration

The measured results of inorganic carbon (Table 2) indicated that the carbon sequestration caused by T_{ERW} in three regions was between 1.22 and 2.80 t-CO_2 ha^{-1} yr^{-1}, but only the semi-humid and humid regions had significant statistical significance ($p < 0.05$). The T_C sequestration in the semi-humid region was 1.63 ± 1,17 t-CO_2 ha^{-1} yr^{-1}, and TIC sequestration was 1.36 ± 0.86 t-CO_2 ha^{-1} yr^{-1} ($p < 0.05$). The total carbon sequestration in our humid region was mainly DIC, with a total of 2.8 ± 0.90 t-CO_2 ha^{-1} yr^{-1}, and DIC accounted for 65.7 ± 39.3 % ($p < 0.01$). Comparing the sequestration amount of inorganic carbon and organic carbon (*Fig. S10*), it was found that the former was 0.68 to 1.5 times greater than the latter.

3.2. Environmental impact factor analysis of farmland ERW

3.2.1. The relative contributions of environmental impact factor

The feature importance of the random forest models was used to determine the relative contributions of environmental factors to the yield, TIC, and DIC changes (Fig. 3a-c). Based on climate, soil, and management factor, the RF model explained 81–89 % (rRMSE = 13.5–18.6 %) predictive variables change.

The factor contribution analysis showed that soil was the dominant aspect affecting the yield increase (51 %), together with the TIC (41 %) and DIC (42 %) accumulation. Contribution analysis of climate factors indicated that precipitation was dramatically more influential than other climate factors, accounting for 10.4, 13.5, and 16.7 % of the changes in yield, TIC, and DIC, respectively. The soil factor contribution analysis showed that the main soil factors affecting ERW yield, DIC, and TIC change included soil pH (9.7–16.8 %) and soil moisture (7–8.2 %). Contribution analysis of management factors showed that the P (7.3 %) and K input 6.6 %) contributed the most to the ERW yield increase. N input (7 and 5.8 %) and rotation (4.2 and 4.3 %) were the greatest contributors to TIC and DIC changes.

3.2.2. The correlation network analysis of impact factor

The correlation network of environmental factors is shown in Fig. 3d-f. The impact factor with the highest correlation to yield change (Fig. 3d) was soil pH ($r = -0.77$, $p < 0.001$), while the other mainly included the soil exchangeable K ($r = -0.65$, $p < 0.001$), exchangeable P ($r = -0.57$, $p < 0.001$), precipitation ($r = 0.54$, $p < 0.001$) and P (r = −0.6, $p < 0.01$), K input ($r = -0.48$, $p < 0.05$). For TIC change (Fig. 3e), the impact factor with the highest correlation was precipitation ($r = 0.61$, $p < 0.01$), and the correlation coefficients r of other factors were all <0.5. For DIC change (Fig. 3f), soil pH was also the most relevant factor ($r = -0.61$, $p < 0.001$), while others mainly included CEC ($r = -0.58$, $p < 0.001$), exchangeable Ca ($r = -0.55$, $p < 0.01$), soil moisture (r = 0.54, $p < 0.001$), precipitation ($r = 0.53$, $p < 0.01$). The matrix of correlation coefficients among all factors is displayed in *Fig. S11*.

3.3. Evaluation of carbon sequestration of ERW in China

3.3.1. Carbon sequestration potential of ERW strategy in different regions

Based on the layout conditions of field experiments (100 t ha^{-1} rock powder every five years and P80 = 38.5 μm), the annual average carbon sequestration. The total carbon sequestration in the whole region reached 441.7 ± 69.3 Mt. yr^{-1}, and carbon sequestration was concentrated in humid areas, accounting for 62.1 % (Table 3), especially in Anhui, Hubei, Hunan, and Jiangxi provinces due to high farmland area and water infiltration (Fig. 4a). The total carbon emission in whole region was 156.9 ± 24.5 Mt. yr^{-1}. The proportion of processing emissions was the highest, up to 74.7 % (Table 3). Detailed data on carbon emissions are summarized in *Table S7*. High carbon emitting farmland was concentrated in the Northeast region, mainly in Heilongjiang and Jilin provinces, due to the less approved rock sources for mining at present

(Fig. 4b). The net carbon sequestration of ERW in the whole region was 284.8 ± 93.8 Mt. yr^{-1} (Table 3). The spatial trend of net sequestration was consistent with that of total carbon sequestration, concentrated in humid areas (67.2 %) (Fig. 4c), and >50 % of farmland net carbon sequestration rates exceed 1.73 t-CO_2 ha^{-1} yr^{-1}.

The sequestration cost of ERW in the whole region ranged from 300 to 1500 CNY ¥ t-CO_2^{-1} (equivalent to 43.6 to 218 US $), with an average of 632.9 ± 161.1 CNY ¥ t-CO_2^{-1} (Table 3). The spatial distribution showed that the sequestration cost of the humid region was lower due to higher net sequestration (Fig. 4d). The frequency distribution indicated that the median of carbon emissions was 643 CNY ¥ t-CO_2^{-1}.

3.3.2. Scenario analysis

Net carbon sequestration was further evaluated under different application rates, particle sizes, electricity emission factors, and transportation methods. Overall, net carbon sequestration was more sensitive to changes in particle size and electricity emission factors (Fig. 5).

As the application amount decreases, the net carbon sequestration also substantially decreased. Under the scenarios of 50 and 25 t ha^{-1} (every five years), the net carbon sequestration in the whole region was 159.7 and 87.1 Mt. yr^{-1}, respectively (Fig. 5a, b). The comparison of different particle sizes showed that a 5-fold increase in P80 increased carbon sequestration by 33 %, while the finer particle sizes (5-fold reduction) resulted in a decrease of 8.2 % (Fig. 5c, d). This indicated that the secondary emissions caused by grinding were higher than the positive benefits brought by the increase in specific surface area of rock powder at the pessimistic energy policy. The statistics based on EFBM further emphasized the importance of energy policies for ERW deployment. Under optimistic electricity emission factors, the net carbon sequestration of ERW in the whole region increased by 42.6 % (Fig. 5e). The impact of different transportation methods on net carbon sequestration was relatively low. In the scenarios of railways, medium diesel, and heavy gasoline trucks, the net carbon sequestration changed by 5.7, −8.6, and − 2.1 %, respectively (Fig. 5f-h).

4. Discussion

4.1. Comparison of field experiment results and other research

The results of crop yield indicated that farmland ERW supports the

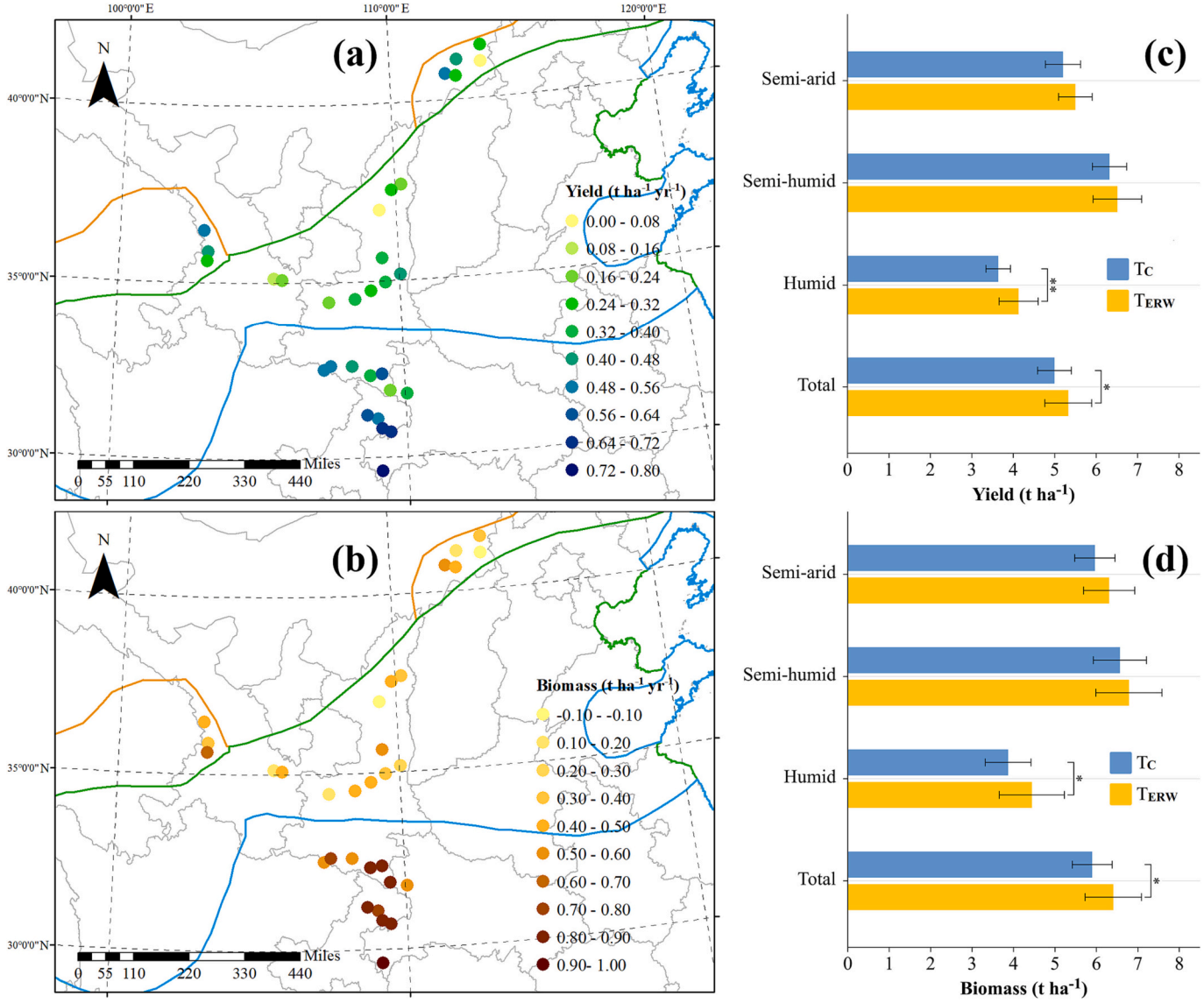

Fig. 2. The annual average yield and biomass change distribution (a, b) and the comparison of the control treatment (T_C) and enhanced rock weathering treatment (T_{ERW}) on crop yield (c) and biomass (d) in the semi-arid, semi-humid, humid and the whole region, respectively. * denote $p < 0.05$, ** is $p < 0.01$ and *** represent $p < 0.001$.

Table 2
Soil, leachate biogeochemistry changes and carbon capture caused by enhanced rock weathering (ERW).

Region		Semi-arid	Semi-humid	Humid
Soil Biogeochemistry change	pH_{soil} (yr^{-1})	0.02 ± 0.08	0.08 ± 0.15	*0.17 ± 0.13
	Exc-P (kg $ha^{-1}yr^{-1}$)	0.98 ± 2.11	−0.32 ± 1.73	**5.71 ± 1.92
	Exc-K (kg $ha^{-1}yr^{-1}$)	3.6 ± 24.2	7.7 ± 28.7	*34.1 ± 20.5
	Exc-Ca (kg $ha^{-1}yr^{-1}$)	383.0 ± 468.3	521.2 ± 483.6	***993.3 ± 205.9
	Exc-Mg (kg $ha^{-1}yr^{-1}$)	*545.2 ± 278.1	**630.7 ± 141.9	***1038.6 ± 102.7
	Exc-Si (kg $ha^{-1}yr^{-1}$)	**64.8 ± 16.0	*87.4 ± 23.2	**97.8 ± 33.1
Leachate chemistry change	$pH_{leachate}$ (yr^{-1})	0.04 ± 0.07	*0.13 ± 0.06	*0.24 ± 0.08
	Lea-Ca (kg $ha^{-1}yr^{-1}$)	34.5 ± 129.2	92.7 ± 123.2	**427.3 ± 119.2
	Lea-Mg (kg $ha^{-1}yr^{-1}$)	18.3 ± 42.9	*56.5 ± 28.3	**279.5 ± 35.4
	Lea-Si (kg $ha^{-1}yr^{-1}$)	−3.93 ± 16.2	3.9 ± 13.7	17.9 ± 33.8
Carbon capture by ERW	TIC (t-CO_2 $ha^{-1}yr^{-1}$)	1.13 ± 1.52	*1.36 ± 0.86	*0.96 ± 0.47
	DIC (t-CO_2 $ha^{-1}yr^{-1}$)	0.09 ± 0.13	0.27 ± 0.31	**1.84 ± 0.43

Note: Exc- is the soil exchange state, and Lea- denotes the dissolved state in leachate. Carbon capture included the change of total soil inorganic carbon (TIC) in the 0-40 cm soil layer and the dissolved inorganic carbon (DIC) leached to the 40-200 cm soil layer.

sustainable goals of the Paris Agreement and can promote climate adaptation and low GHG emissions development in a way that does not threaten food production (Beerling et al., 2018; Lefebvre et al., 2019; Rinder and Hagke, 2021; Swoboda et al., 2021). In humid areas, ERW on farmland was also an effective management strategy that maximized agricultural sustainability and resource co-benefits by improving crop yield (13.5 ± 5.2 %) and replacing lime and part chemical fertilizers (Plata et al., 2021). Haque et al. (2019) reported a substantial yield increase for corn and soybean (90 and 177 %) in wollastonite-amended (221 %) acidic soils. Therefore, ERW has taken on a more attractive function in more targeted soils or crops. However, the yield increase reported was mostly <30 % in conventional farmland, such as 21 ± 9.4 % in sorghum yield (Kelland et al., 2020), 15.6 % in ryegrass biomass (ten Berge et al., 2012), and 18.4 % in wheat grain (Rudmin et al., 2019), all of which were close to our results.

T_{ERW} significantly increased ($p < 0.05$) soil pH by 0.17 ± 0.13 yr^{-1} in the humid region (Fig. 2), which was beneficial for inhibiting Al toxicity and improving nutrient availability (Malik et al., 2018; Haque et al., 2019; Mi et al., 2019; Dang et al., 2022). In general, the interference ability of silicate rocks on soil pH was lower than that of carbonate rocks (Harvey, 2008; Zeng et al., 2022). Dietzen et al., 2018reported that in a three-month soil culture experiment, lime increased the pH of strongly acidic soil (pH = 3.56) by 2.51 units, while olivine only increased by 1.13–1.63. However, the reaction between carbonates and soil acidic substances can cause CO_2 to return to the atmosphere, as well as the latter does not contain the beneficial element Si (Hartmann et al., 2013; Dietzen et al., 2018; Kelland et al., 2020). Adequate soil availability Si was beneficial for improving crop resistance to diseases, pests, toxic elements, and drought (Adrees et al., 2015; Liu et al., 2017; Dietzen et al., 2018; Rinder and Hagke, 2021). For high-demand Si crops such as rice, it was necessary to regularly apply Si fertilizer to compensate for the loss of soil Si (Ma, 2004; Sun et al., 2019). The vast majority of studies on the soil improvement with silicate rock powder had reported an increase in soil Si (Swoboda et al., 2021), this study also showed that Si has been significantly improved (7.8–14.2 %) in all climatic regions.

The Mg dissolution was an important index for assessing the minerals weathering because Mg was present in comparatively active minerals, and was less affected by plant uptake and secondary precipitation than Ca (Kelland et al., 2020). The Mg dissolution rate of mixed rock powder was roughly calculated based on the changes in the soil exchangeable pool and leachate, which were 10^{-12}, $10^{-12.2}$, and $10^{-12.3}$ mol m^{-2} s^{-1} in semi-arid, semi-humid, and humid, respectively. These results were close to the Mg release rates ($10^{-11.8}$ -$10^{-13.7}$) of ultrabasic (olivine) and basic (basalt) rock in mesoscale experiments (Renforth et al., 2015; Amann et al., 2020; Kelland et al., 2020).

Due to the different trial preconditions (rock dosage, particle size, duration, etc.) and statistical methods, carbon sequestration rates in prior studies ranged from 0.023 to 39.3 t-CO_2 ha^{-1} (0.10×10^{-3} to 0.31 t-CO_2 $t\text{-}rock^{-1}$) (ten Berge et al., 2012; Dietzen et al., 2018; Haque et al., 2019; Amann et al., 2020; Kelland et al., 2020; Swoboda et al., 2021). Under the uniform rock types and modification conditions, the carbon sequestration caused by ERW in semi-arid, semi-humid, and humid regions reached 1.2, 1.6, and 2.8 t-CO_2 ha^{-1} yr^{-1} (0.039, 0.052 and 0.09 t-CO_2 $t\text{-}rock^{-1}$ yr^{-1}) (Table 2), which were similar to the unit mass weathering rate of basalt (0.024–0.03 t-CO_2 $t\text{-}rock^{-1}$ yr^{-1}) and olivine (0.021–0.287 $t\text{-}rock^{-1}$ yr^{-1}) in the mesoscale experiment (ten Berge et al., 2012; Kelland et al., 2020).

4.2. Evaluating of driving factors for yield and carbon sequestration change

Contribution analysis and correlation networks both indicated that precipitation and soil pH were the dominant factors affecting ERW yield and carbon sequestration change (Fig. 3). The importance of precipitation and soil pH has been emphasized in silicate natural feedback (Maher, 2010; Swoboda et al., 2021; Zhang et al., 2021), they were also critical factors affecting pedogenic carbonate accumulation (Zamanian et al., 2016; Zeng et al., 2022). Precipitation controlled the localization of weathering product by affecting the depth of leaching accumulation, carbonate supersaturation, soil respiration, and evapotranspiration (Borchardt and Lienkaemper, 1999; Eswaran et al., 2000; Retallack, 2005; Khormali et al., 2012). Precipitation renewed various chemical balances in soil water, and reduced carbonate saturation in soil pores, thereby increasing the chemical difference between the soil water and the surface of rock particles (Goudie and Viles, 2012; Shi et al., 2012; Anda et al., 2013). Soil pH directly reflected the type (H_2O or H^+) and magnitude of catalytic media in the rock weathering environment (Palandri and Kharaka, 2004; Cipolla et al., 2021). Seriously insufficient reserves of weatherable minerals and their soluble weathering products in acid or strongly acid soil also accelerated the rapid dissolution of exogenous silicate rock powder (Hartmann et al., 2013; Zamanian et al., 2016; Swoboda et al., 2021).

Contribution analysis (Fig. 3) also demonstrated that management factors had a non-negligible impact on the farmland ERW (24–26.2 %). Fertilizer and irrigation were directly related to yield and soil inorganic carbon changes. P and K inputs play an important role in ERW yield increase by controlling the available nutrients in the soil. For sites with low P and K inputs, the potential for ERW to increase yield was considerable. N input contributed considerably to changes in TIC and DIC because a large amount of N input was able to provide additional active H^+ for farmland soil (Monger and Kraimer, 2015; Zamanian et al., 2018; Raza et al., 2020; Koester et al., 2021). Organic fertilizer can add organic acids to the soil and provide various organic colloids that increase the solubility of soil base ions (Eswaran et al., 2000). Previous

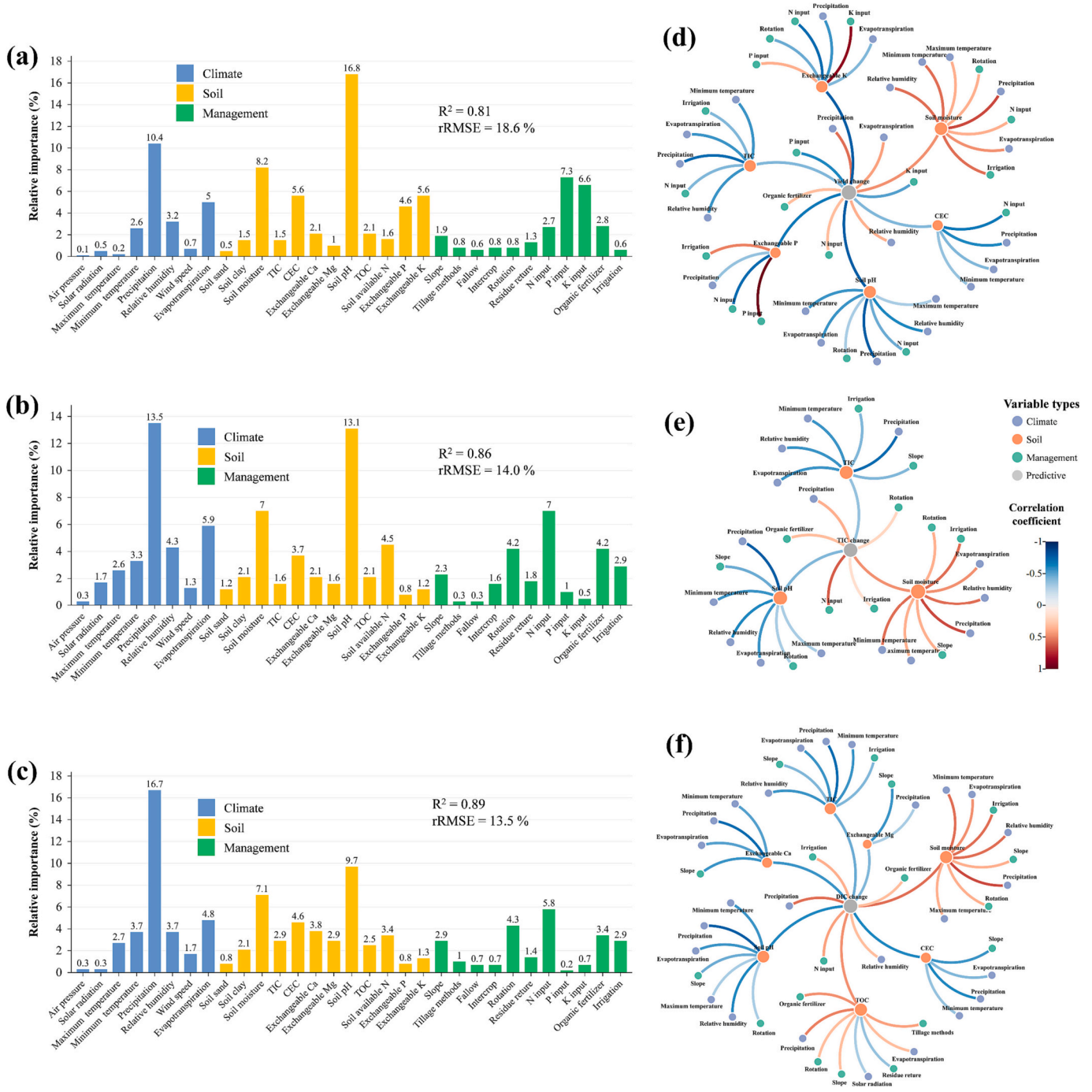

Fig. 3. Relative contributions (a, b, c) and correlation coefficient network (d, e, f) of climate, soil, and management factors to the changes of yield, total soil inorganic carbon (TIC), and dissolved inorganic carbon (DIC).

experiments had also shown that the combined application of rock powder and organic materials (such as compost and manure) accelerated K release (de Souza et al., 2018) and SIC accumulation (Manning et al., 2013). Crop rotation in this study referred to planting winter wheat from November to May. The planting of winter wheat not only increased fertilizer and irrigation input but also provided a longer rhizosphere effect to the rock dissolution, which had clear effects on the TIC and DIC change (Fig. 3). Irrigation ranked fourth in its management contribution to changes in DIC and TIC. Similar to precipitation, timely irrigation can adjust the chemical state of soil moisture and relieve the supersaturated state of salt bases in the soil aqueous solution (Hartmann et al., 2013).

4.3. Potential and feasibility of enhanced rock weathering in Chinese farmland

Simulation analysis of three regions in China showed that ERW can capture nearly 0.28 Gt CO_2 per year (Table 3). If the simulation is considered on an optimistic energy policy basis, net carbon sequestration could reach 0.40 Gt CO_2 per year (Fig. 4). Furthermore, this value will be more attractive. if the application rate or frequency is promoted. Beerling et al. (2020) evaluated that farmland enhanced basalt weathering in China could sequester 0.13 to 0.52 Gt CO_2 yr^{-1} (application area from 10 to 55 %) at an application rate of 40 t ha^{-1} yr^{-1} (equivalent to twice the amount of this experiment). The discrepancy may be due to

Table 3
Carbon sequestration potential and sequestration cost statistics in three climate regions of China.

Region		Semi-arid	Semi-Humid	Humid	Whole
Carbon sequestration ($Mt\text{-}CO_2\ yr^{-1}$)	TIC	14.0 ± 2.3	63.6 ± 4.4	85.2 ± 19.9	162.9 ± 26.6
	DIC	10.7 ± 1.2	79.4 ± 9.1	188.9 ± 32.4	278.9 ± 42.7
	TC	24.6 ± 3.5	143.0 ± 13.5	274.1 ± 52.3	441.7 ± 69.3
Carbon emission ($Mt\text{-}CO_2\ yr^{-1}$)	Mining	0.8 ± 0.03	3.9 ± 0.4	5.3 ± 0.6	10.0 ± 1.1
	Processing	9.3 ± 0.4	46.1 ± 4.9	61.8 ± 7.0	117.2 ± 12.3
	Transport	2.3 ± 1.0	9.9 ± 3.3	13.2 ± 5.7	25.4 ± 10
	Application	0.3 ± 0.2	1.6 ± 0.4	2.4 ± 0.5	4.3 ± 1.1
	Total	12.7 ± 1.6	61.5 ± 9.0	82.7 ± 13.8	156.9 ± 24.5
Net sequestration ($Mt\ yr^{-1}$)		11.9 ± 5.1	81.5 ± 22.5	191.4 ± 66.1	284.8 ± 93.8
Sequestration cost (CNY ¥ $t\text{-}CO_2^{-1}$)		707.9 ± 119.4	733.0 ± 139.2	553.7 ± 147.1	632.9 ± 161.1

Note: TIC was the carbon sequestration by soil inorganic carbon in 0-40 cm soil layer, DIC denotes the carbon sequestration with dissolved inorganic carbon in leachate below 40 cm soil layer, and TC is total carbon sequestration.

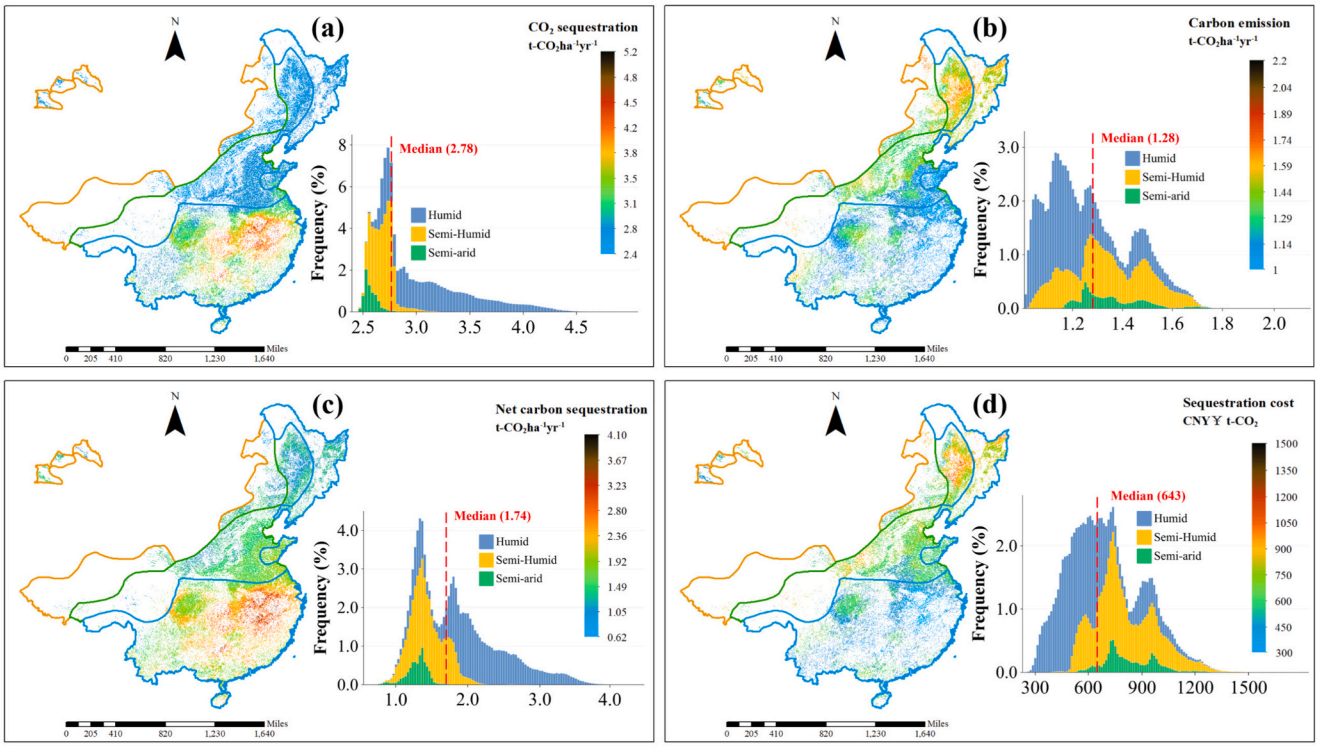

Fig. 4. The spatial distribution of annual average carbon sequestration (a), carbon emissions (b), net carbon sequestration (c), and sequestration cost (d) to enhance rock weathering during 20 years in China. The rock application rate was 100 t-rock every five years, The P80 of rock particle was set at 38.5 μm.

different rock mineralogy, more conservative and pessimistic energy policies, and the farmland in the arid region was not considered. The deployment of the ERW strategy resulted in secondary emissions of 0.16 Gt yr^{-1}, with processing accounting for the highest proportion, exceeding 74.7 % (Table 3). After increasing the P80 of the rock powder by five times, it was found that the net sequestration increased by 33 % (Fig. 5), which indicated that under pessimistic energy policies, the secondary emissions generated by grinding were higher than the positive benefits brought about by the increase in the specific surface area of rock powder. It can be seen that finer particle sizes (namely faster sequestration effects) required cleaner energy policies to support.

The sequestration cost of farmland ERW was 632.9 ± 161 CNY ¥ $t\text{-}CO_2^{-1}$ (92 ± 23.4 US $ $t\text{-}CO_2^{-1}$), which was slightly lower than BECCS (100–200 US $ $t\text{-}CO_2^{-1}$) and direct air capture and storage (100–300 US $ $t\text{-}CO_2^{-1}$), but remain higher than China's currently large-scale development soil organic carbon sequestration (0–10 US $ $t\text{-}CO_2^{-1}$) and greening engineering (< 100 US $ $t\text{-}CO_2^{-1}$) (Fuss et al., 2018; Strefler et al., 2018; Beerling et al., 2020; Yin et al., 2022). However, compared to large-scale greening projects, ERW technology will not compete for land resources with farmland, and it can be co-configured with various strategies mentioned above for carbon sequestration (Amann and Hartmann, 2019; Rinder and Hagke, 2021). In addition, the following scenarios may make the deployment cost of farmland ERW more attractive and market competitive: (1) replacing lime to control large area soil acidification in humid regions of China and reduce the secondary emissions from the lime industry, which accounted for up to 15 % of the total greenhouse gas emissions of China (Shan et al., 2016); (2) as slow-release fertilizer in paddy soil to replace part expensive water-soluble silicon fertilizer (Chen et al., 2011); (3) providing natural mineral nutrients for 2 million hectares of organic agriculture in China (FiBL and IFOAM, 2014); (4) reducing costs through the reuse of a large amount of silicate waste rocks, tailings, or artificial waste resources; and (5) higher carbon trading prices were predicted in the future. According to World Bank predicted, the price of carbon trading will reach 100–150 US $ $t\text{-}CO_2^{-1}$ in 2050 (Beerling et al., 2020). However, the specific ERW strategies for any purpose require conducting experiments in advance to assess their potential and risks.

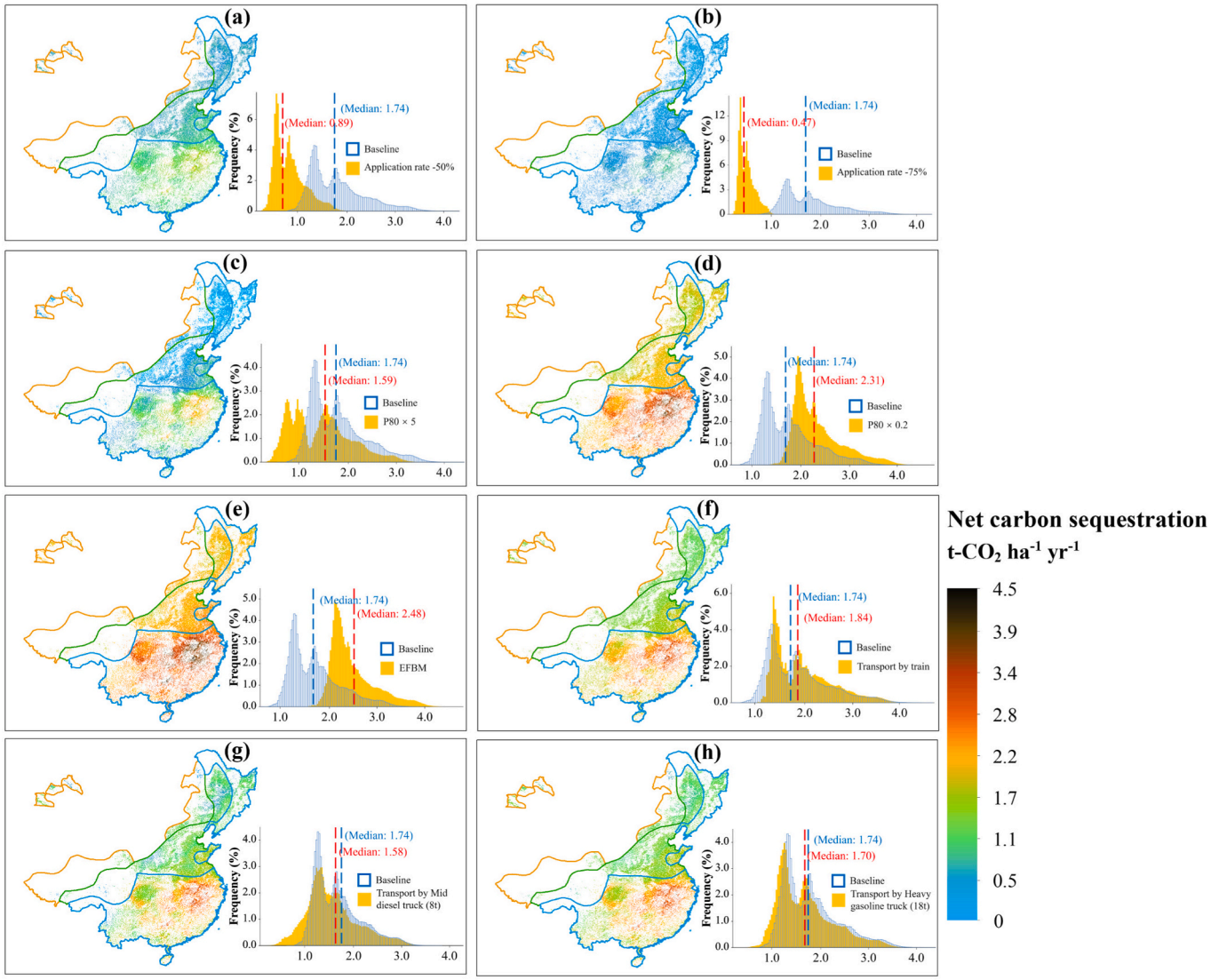

Fig. 5. The spatial distribution of annual average net carbon sequestration in different application rates, rock particle sizes, electricity emission factors, and transport types. In the baseline, the application rate was 100 t-rock every five years, P80 = 38.5 μm, Electricity emission factor was operation margin (EFOM) and transport was heavy diesel truck (Loat 30 t). P80 denotes the rock mass ratio with particle size less than this value reached 80 %. EFBM is the electricity emission factor of the build margin.

4.4. Uncertainty analysis

For field monitoring experiments, the stability and persistence of TIC and DIC required to be further evaluated through a longer-term observation. TIC in soil surface may dissolve to form DIC or form CO_2 again, which can affect the quantification of carbon sequestration. Moreover, the carbon sequestration measured in this experiment was only a snapshot of the total carbon sequestration of ERW. Due to the slow dissolution rate, minerals will still capture carbon for a long time in the future, especially in semi-arid region (observed only for one year).

For simulation analysis, the most uncertain factor came from the diversity of rock mineralogy. Further large-scale surveys were required to grasp the mineral composition and elemental content of silicate rocks in different regions of China to further quantify sequestration potential and risks. Reasonable rock application rates also required further determination through conducting relevant field experiments for different purposes. The amorphous silicon-rich surface formed during the dissolution process of rocks can cause passivation and inhibit the weathering process. The lack of a detailed description of this process also brings some uncertainty to the simulation analysis (Beerling et al., 2020). Furthermore, as indicated by the analysis of impact factors, further experiments are required to quantify the impact of different farmland management methods, especially fertilization.

5. Conclusion

The yield benefits and carbon sequestration potential of farmland ERW were analyzed in the semi-arid, semi-humid, and humid region of China with unified minerals types and particle distributions. The results demonstrated that farmland ERW can improve crop yield, soil pH, and multi-nutrient effectiveness in a wider range of subtropical and temperate farmland. The carbon sequestration of farmland ERW in China was substantial, up to 0.28–0.40 Gt yr^{-1}, which had the potential to contribute to agricultural carbon neutralization. This study provided more detailed field data for farmland ERW under different climatic conditions, which contributed to quantifying the relationship between multiple environmental factors and rock weathering. However, it is crucial to note that the stability and persistence of the sequestration phase require a more extended monitoring period to be adequately assessed. The field benefits of rock powder were driven by precipitation

and soil pH, but management factors, such as fertilization, also played an important role. Further experiments are yet required to find definitive evidence that field management accelerates rock weathering and effective means of quantifying these effects.

Declaration of competing interest

The authors declare that they have no known competing financial interests or personal relationships that could have appeared to influence the work reported in this paper.

Data availability

Data will be made available on request.

Acknowledgment

We acknowledged the support of the National Natural Science Foundation of China (grant numbers: 42077325, 41571218, 41401613) for this study. We are grateful to several field experiment demonstration stations, including Fuping and Ansai, for providing and managing sample plots. Thanks to the Resource and Environment Science and Data Center and National Meteorological Information Center for the provision of soil and climate data. Thanks to Ph.D. Mukesh Kumar Awasthi for improving the English language of the manuscript. We are also sincerely grateful to two anonymous reviewers for their comments on the manuscript.

Appendix A. Supplementary data

Supplementary data to this article can be found online at https://doi.org/10.1016/j.scitotenv.2023.166118.

References

Adrees, M., Ali, S., Rizwan, M., Zia-ur-Rehman, M., Ibrahim, M., Abbas, F., Farid, M., Qayyum, M.F., Irshad, M.K., 2015. Mechanisms of silicon-mediated alleviation of heavy metal toxicity in plants: a review. Ecotoxicol. Environ. Saf. 119, 186–197. https://doi.org/10.1016/j.ecoenv.2015.05.011.

Allen, R.G., Pereira, L.S., Raes, D., Smith, M., 1998. Crop Evapotranspiration-Guidelines for Computing Crop Water Requirements. FAO Irrigation and Drainage Paper 56 300 (9). FAO, Rome, Italia, p. D05109.

Amann, T., Hartmann, J., 2019. Ideas and perspectives: synergies from co-deployment of negative emission technologies. Biogeosciences 16, 2949–2960. https://doi.org/10.5194/bg-16-2949-2019.

Amann, T., Hartmann, J., Struyf, E., Garcia, W.D.O., Schoelynck, J., 2020. Enhanced weathering and related element fluxes-a cropland mesocosm approach. Biogeosciences 17, 103–119. https://doi.org/10.5194/bg-17-103-2020.

Anda, M., Shamshuddin, J., Fauziah, C.I., 2013. Increasing negative charge and nutrient contents of a highly weathered soil using basalt and rice husk to promote cocoa growth under field conditions. Soil Till. Res. 132, 1–11. https://doi.org/10.1016/j.still.2013.04.005.

Arriaga, F.J., Lowery, B., Mays, M.D., 2006. A fast method for determining soil particle size distribution using a laser instrument. Soil Sci. 171, 663–674. https://doi.org/10.1097/01.ss.0000228056.92839.88.

Bao, S., 2000. Agrochemical Analysis of Soil. China Agriculture Press, Beijing.

Beerling, D.J., Leake, J.R., Long, S.P., Scholes, J.D., Ton, J., Nelson, P.N., Bird, M., Kantzas, E., Taylor, L.L., Sarkar, B., Kelland, M., DeLucia, E., Kantola, I., Müller, C., Rau, G., Hansen, J., 2018. Farming with crops and rocks to address global climate, food and soil security. Nat. Plants 4, 138–147. https://doi.org/10.1038/s41477-018-0108-y.

Beerling, D.J., Kantzas, E.P., Lomas, M.R., Wade, P., Eufrasio, R.M., Renforth, P., Sarkar, B., Andrews, M.G., James, R.H., Pearce, C.R., Mercure, J.F., Pollitt, H., Holden, P.B., Edwards, N.R., Khanna, M., Koh, L., Quegan, S., Pidgeon, N.F., Janssens, I.A., Hansen, J., Banwart, S.A., 2020. Potential for large-scale CO_2 removal via enhanced rock weathering with croplands. Nature 583, 242–248. https://doi.org/10.1038/s41586-020-2448-9.

ten Berge, H.F.M., Hugo, G.V.D.M., Johan, W.S., Paul, W.G., Knops, P., Verhagen, J., 2012. Olivine weathering in soil, and its effects on growth and nutrient uptake in ryegrass (Loliumperenne L.): a pot experiment. PLoS One 7, e42098. https://doi.org/10.1371/journal.pone.0042098.

Borchardt, G., Lienkaemper, J.J., 1999. Pedogenic calcite as evidence for an early Holocene dry period in the San Francisco Bay area, California. Geol. Soc. Am. Bull. 111, 906–918. https://doi.org/10.1130/0016-7606(1999)111<0906:PCAEFA>2.3.CO;2.

Brantley, S.L., Kubicki, J.D., White, A.F., 2008. Kinetics of Water-Rock Interaction. Springer, New York, NY. https://doi.org/10.1007/978-0-387-73563-4

Breiman, L., 2001. Random forests. Mach. Learn. 45, 5–32. https://doi.org/10.1023/a:1010933404324.

Brunauer, S., Emmett, P.H., Teller, E., 1938. Adsorption of gases in multimolecular layers. J. Am. Chem. Soc. 60, 309–319. https://doi.org/10.1021/ja01269a023.

Chen, W., Yao, X., Cai, K., Chen, J., 2011. Silicon alleviates drought stress of rice plants by improving plant water status, photosynthesis and mineral nutrient absorption. Biol. Trace Elem. Res. 142, 67–76. https://doi.org/10.1007/s12011-010-8742-x.

Chung, F.H., 1974. A new X-ray diffraction method for quantitative multicomponent analysis. Adv. X-ray Anal. 17, 106–115. https://doi.org/10.1154/s0376030800005231.

Cipolla, G., Calabrese, S., Noto, L.V., Porporato, A., 2021. The role of hydrology on enhanced weathering for carbon sequestration I. modeling rock-dissolution reactions coupled to plant, soil moisture, and carbon dynamics. Adv. Water Resour. 154, 103934 https://doi.org/10.1016/j.advwatres.2021.103934.

Dalmora, A.C., Ramos, C.G., Silva Oliveira, M.L., Silva Oliveira, L.F., Homrich Schneider, I.A., Kautzmann, R.M., 2020. Application of andesite rock as a clean source of fertilizer for eucalyptus crop: evidence of sustainability. J. Clean. Prod. 256, 120432 https://doi.org/10.1016/j.jclepro.2020.120432.

Dang, C., Kong, F., Li, Y., Jiang, Z., Xi, M., 2022. Soil inorganic carbon dynamic change mediated by anthropogenic activities: an integrated study using meta-analysis and random forest model. Sci. Total Environ. 835, 155463 https://doi.org/10.1016/j.scitotenv.2022.155463.

Deer, W.A., Howie, R.A., Zussman, J., 2013. An Introduction to the Rock-Forming Minerals, 3rd ed. The Minerological Society, London.

Dietzen, C., Harrison, R., Michelsen-Correa, S., 2018. Effectiveness of enhanced mineral weathering as a carbon sequestration tool and alternative to agricultural lime: an incubation experiment. Int. J. Greenh. Gas Con. 74, 251–258. https://doi.org/10.1016/j.ijggc.2018.05.007.

Dong, W., Duan, Y., Wang, Y., Hu, C., 2016. Reassessing carbon sequestration in the North China plain via addition of nitrogen. Sci. Total Environ. 563–564, 138–144. https://doi.org/10.1016/j.scitotenv.2016.04.115.

Elith, J., Leathwick, J.R., Hastie, T., 2008. A working guide to boosted regression trees. J. Anim. Ecol. 77, 802–813. https://doi.org/10.1111/j.1365-2656.2008.01390.x.

Eswaran, H., Reich, P.F., Kimble, J.M., Beinroth, F.H., Padmanabhan, E.M.P., 2000. Global carbon stocks. In: Lal, R., Kimble, J.M., Eswaran, H., Stewart, B.A. (Eds.), Global Climate Change and Pedogenic Carbonates. CRC Press, Boca Raton, Fla, pp. 15–25. https://doi.org/10.1016/S0016-7061(01)00059-3.

FiBL, IFOAM, 2014. The world of organic agriculture: Statistics & Emerging trends 2014. Nuremberg: Bio. Fach. Congress. https://www.fibl.org/fileadmin/documents/shop/1636-organic-world-2014.pdf.

Fu, S., Zou, J., Liu, L., 2015. An analysis of China's INDC. China National Center for climate change strategy and international cooperation (NCSC). http://www.chinacarbon.info/wp-content/uploads/2015/07/Comments-on-Chinas-INDC.pdf.

Fuss, S., Lamb, W.F., Callaghan, M.W., Hilaire, J., Creutzig, F., Amann, T., Beringer, T., de Oliveira Garcia, W., Hartmann, J., Khanna, T., Luderer, G., Nemet, G.F., Rogelj, J., Smith, P., Vicente, J.L.V., Wilcox, J., del Mar Zamora Dominguez, M., Minx, J.C., 2018. Negative emissions—part 2: costs, potentials and side effects. Environ. Res. Lett. 13, 063002 https://doi.org/10.1088/1748-9326/aabf9f.

Gai, X., Liu, H., Liu, J., Zhai, L., Yang, B., Wu, S., Ren, T., Lei, Q., Wang, H., 2018. Long-term benefits of combining chemical fertilizer and manure applications on crop yields and soil carbon and nitrogen stocks in North China plain. Agric. Water Manag. 208, 384–392. https://doi.org/10.1016/j.agwat.2018.07.002.

Gong, J.Y., 2000. Statistical Methods for Experiment. China Agriculture Press, Beijing.

Goudie, A.S., Viles, H.A., 2012. Weathering and the global carbon cycle: geomorphological perspectives. Earth-Sci. Rev. 113, 59–71. https://doi.org/10.1016/j.earscirev.2012.03.005.

Guo, F., Wang, Y., Zhu, H., Zhang, C., Sun, H., Fang, Z., Yang, J., Zhang, L., Mu, Y., Man, Y.B., Wu, F., 2023. Crop productivity and soil inorganic carbon change mediated by enhanced rock weathering in farmland: a comparative field analysis of multi-agroclimatic regions in Central China. Agric. Syst. 210, 103691 https://doi.org/10.1016/j.agsy.2023.103691.

Han, X., Gao, G., Chang, R., Li, Z., Ma, Y., Wang, S., Wang, C., Lü, Y., Fu, B., 2018. Changes in soil organic and inorganic carbon stocks in deep profiles following cropland abandonment along a precipitation gradient across the loess plateau of China. Agric. Ecosyst. Environ. 258, 1–13. https://doi.org/10.1016/j.agee.2018.02.006.

Hao, T., Zhu, Q., Zeng, M., Shen, J., Shi, X., Liu, X., Zhang, F., de Vries, W., 2018. Quantification of the contribution of nitrogen fertilization and crop harvesting to soil acidification in a wheat-maize double cropping system. Plant Soil 434, 167–184. https://doi.org/10.1007/s11104-018-3760-0.

Haque, F., Santos, R.M., Dutta, A., Thimmanagari, M., Chiang, Y.W., 2019. Co-benefits of wollastonite weathering in agriculture: CO_2 sequestration and promoted plant growth. ACS Omega 4, 1425–1433. https://doi.org/10.1021/acsomega.8b02477.

Haque, F., Santos, R.M., Chiang, Y.W., 2020. CO_2 sequestration by wollastonite-amended agricultural soils-an Ontario field study. Int. J. Greenh. Gas Con. 97, 103017 https://doi.org/10.1016/j.ijggc.2020.103017.

Hartmann, J., West, A.J., Renforth, P., Köhler, P., Rocha, C.L.D.L., Wolf-Gladrow, D.A., Dürr, H.H., Scheffran, J., 2013. Enhanced chemical weathering as a geoengineering strategy to reduce atmospheric carbon dioxide, supply nutrients, and mitigate ocean acidification. Rev. Geophys. 51, 113–149. https://doi.org/10.1002/rog.20004.

Harvey, L.D.D., 2008. Mitigating the atmospheric CO_2 increase and ocean acidification by adding limestone powder to upwelling regions. J. Geophys. Res. 113 https://doi.org/10.1029/2007jc004373.

Jariwala, H., Haque, F., Vanderburgt, S., Santos, R.M., Chiang, Y.W., 2022. Mineral-soil-plant-nutrient synergisms of enhanced weathering for agriculture: short-term investigations using fast-weathering wollastonite skarn. Front. Plant Sci. 13, 929457 https://doi.org/10.3389/fpls.2022.929457.

Kelland, M.E., Wade, P.W., Lewis, A.L., Taylor, L.L., Sarkar, B., Andrews, M.G., Lomas, M.R., Cotton, T.E.A., Kemp, S.J., James, R.H., Pearce, C.R., Hartley, S.E., Hodson, M.E., Leake, J.R., Banwart, S.A., Beerling, D.J., 2020. Increased yield and CO_2 sequestration potential with the C_4 cereal Sorghum bicolor cultivated in basaltic rock dust-amended agricultural soil. Glob. Chang. Biol. 26, 3658–3676. https://doi.org/10.1111/gcb.15089.

Khormali, F., Ghergherechi, S., Kehl, M., Ayoubi, S., 2012. Soil formation in loess-derived soils along a subhumid to humid climate gradient, northeastern Iran. Geoderma 179–180, 113–122. https://doi.org/10.1016/j.geoderma.2012.02.002.

Koester, M., Stock, S.C., Nájera, F., Abdallah, K., Gorbushina, A., Prietzel, J., Matus, F., Klysubun, W., Boy, J., Kuzyakov, Y., Dippold, M.A., Spielvogel, S., 2021. From rock eating to vegetarian ecosystems-disentangling processes of phosphorus acquisition across biomes. Geoderma 388, 114827. https://doi.org/10.1016/j.geoderma.2020.114827.

Köhler, P., Hartmann, J., Wolf-Gladrow, D.A., 2010. Geoengineering potential of artificially enhanced silicate weathering of olivine. Proc. Natl. Acad. Sci. 107, 20228–20233. https://doi.org/10.1073/pnas.1000545107.

Lefebvre, D., Goglio, P., Williams, A., Manning, D.A.C., de Azevedo, A.C., Bergmann, M., Meersmans, J., Smith, P., 2019. Assessing the potential of soil carbonation and enhanced weathering through life cycle assessment: a case study for Sao Paulo State, Brazil. J. Clean. Prod. 233, 468–481. https://doi.org/10.1016/j.jclepro.2019.06.099.

Leroux, L., Faye, N.F., Jahel, C., Falconnier, G.N., Diouf, A.A., Ndao, B., Tiaw, I., Senghor, Y., Kanfany, G., Balde, A., Dieye, M., Sirdey, N., Loison, S.A., Corbeels, M., Baudron, F., Bouquet, E., 2022. Exploring the agricultural landscape diversity-food security nexus: an analysis in two contrasted parklands of Central Senegal. Agric. Syst. 196, 103312 https://doi.org/10.1016/j.agsy.2021.103312.

Li, L., Wang, B., Feng, P., Wang, H., He, Q., Wang, Y., Liu, D.L., Li, Y., He, J., Feng, H., Yang, G., Yu, Q., 2021. Crop yield forecasting and associated optimum lead time analysis based on multi-source environmental data across China. Agric. For. Meteorol. 308–309, 108558 https://doi.org/10.1016/j.agrformet.2021.108558.

Li, Y.S., 1983. The properties of water cycle in soil and their effect on water cycle for land in the loess plateau. Acta Ecol. Sin. 3, 91–101. https://kns.cnki.net/kcms/detail/detail.aspx?FileName=STXB198302000&DbName=CJFQ1983.

Li, Z.P., Han, F.X., Su, Y., Zhang, T.L., Sun, B., Monts, D.L., Plodinec, M.J., 2007. Assessment of soil organic and carbonate carbon storage in China. Geoderma 138, 119–126. https://doi.org/10.1016/j.geoderma.2006.11.007.

Liu, S., Qi, X., Han, C., Liu, J., Sheng, X., Li, H., Luo, A., Li, J., 2017. Novel nano-submicron mineral-based soil conditioner for sustainable agricultural development. J. Clean. Prod. 149, 896–903. https://doi.org/10.1016/j.jclepro.2017.02.155.

Ma, J.F., 2004. Role of silicon in enhancing the resistance of plants to biotic and abiotic stresses. Soil Sci. Plant Nutr. 50, 11–18. https://doi.org/10.1080/00380768.2004.10408447.

Maher, K., 2010. The dependence of chemical weathering rates on fluid residence time. Earth Planet. Sc. Lett. 294, 101–110. https://doi.org/10.1016/j.epsl.2010.03.010.

Malik, A.A., Puissant, J., Buckeridge, K.M., Goodall, T., Jehmlich, N., Chowdhury, S., Gweon, H.S., Peyton, J.M., Mason, K.E., van Agtmaal, M., Blaud, A., Clark, I.M., Whitaker, J., Pywell, R.F., Ostle, N., Gleixner, G., Griffiths, R.I., 2018. Land use driven change in soil pH affects microbial carbon cycling processes. Nat. Commun. 9, 3591. https://doi.org/10.1038/s41467-018-05980-1.

Manning, D.A.C., Renforth, P., Lopez-Capel, E., Robertson, S., Ghazireh, N., 2013. Carbonate precipitation in artificial soils produced from basaltic quarry fines and composts: an opportunity for passive carbon sequestration. Int. J. Greenh. Gas Con. 17, 309–317. https://doi.org/10.1016/j.ijggc.2013.05.012.

Mi, W., Sun, Y., Gao, Q., Liu, M., Wu, L., 2019. Changes in humus carbon fractions in paddy soil given different organic amendments and mineral fertilizers. Soil Till. Res. 195, 104421 https://doi.org/10.1016/j.still.2019.104421.

Ming, D.X., 2013. Field Experiment and Statistical Analysis. Science Press, Beijing.

MoA, 2006. NY/T 1121.13-2006: Soil testing part 13: Method for determination of soil exchangeable calcium and magnesium. In: Ministry of Agriculture of the PRC. China Standards Press.

MoA, 2008. NY/T 1615–2008: Determination of Exchangeable Bases and Total Exchangeable Bases in Calcareous Soil. China Standards Press, Ministry of Agriculture of the PRC.

Monger, H.C., Kraimer, R.A., Khresat, S.E., Cole, D.R., Wang, X., Wang, J., 2015. Sequestration of inorganic carbon in soil and groundwater. Geology 43, 375–378. https://doi.org/10.1130/g36449.1.

Moosdorf, N., Renforth, P., Hartmann, J., 2014. Carbon dioxide efficiency of terrestrial enhanced weathering. Environ. Sci. Technol. 48, 4809–4816. https://doi.org/10.1021/es4052022.

NGA, 2019. China Mineralogical Database 2020 Edition. National geological archives (NGA). http://data.ngac.org.cn/mineralresource/index.html?id=302c137ee126465095b3df8e68168d8c.

NMIC, 2017. China Meteorological Administration Land Surface Data Assimilation System (CLDAS-V2.0) near Real-Time Product Dataset. National Meteorological Information Center. http://data.cma.cn/.

Nugroho, A.D., Prasada, I.Y., Lakner, Z., 2023. Comparing the effect of climate change on agricultural competitiveness in developing and developed countries. J. Clean. Prod. 406 https://doi.org/10.1016/j.jclepro.2023.137139.

Palandri, J.L., Kharaka, Y.K., 2004. A Compilation of Rate Parameters of Water-Mineral Interaction Kinetics for Application to Geochemical Modeling. Report No. 2004–1068 (Pp. 1–64). U.S. Geological Survey, Menlo Park, CA.

Penman, D.E., Rugenstein, J.K.C., Ibarra, D.E., Winnick, M.J., 2020. Silicate weathering as a feedback and forcing in Earth's climate and carbon cycle. Earth-Sci. Rev. 209, 103298 https://doi.org/10.1016/j.earscirev.2020.103298.

Plata, L.G., Ramos, C.G., Silva Oliveira, M.L., Silva Oliveira, L.F., 2021. Release kinetics of multi-nutrients from volcanic rock mining by-products: evidences for their use as a soil remineralizer. J. Clean. Prod. 279, 123668 https://doi.org/10.1016/j.jclepro.2020.123668.

Qiu, S., Gao, H., Zhu, P., Hou, Y., Zhao, S., Rong, X., Zhang, Y., He, P., Christie, P., Zhou, W., 2016. Changes in soil carbon and nitrogen pools in a Mollisol after long-term fallow or application of chemical fertilizers, straw or manures. Soil Till. Res. 163, 255–265. https://doi.org/10.1016/j.still.2016.07.002.

Raza, S., Miao, N., Wang, P., Ju, X., Chen, Z., Zhou, J., Kuzyakov, Y., 2020. Dramatic loss of inorganic carbon by nitrogen-induced soil acidification in Chinese croplands. Glob. Chang. Biol. 26, 3738–3751. https://doi.org/10.1111/gcb.15101.

Renforth, P., 2012. The potential of enhanced weathering in the UK. Int. J. Greenh. Gas Con. 10, 229–243. https://doi.org/10.1016/j.ijggc.2012.06.011.

Renforth, P., 2019. The negative emission potential of alkaline materials. Nat. Commun. 10, 1401. https://doi.org/10.1038/s41467-019-09475-5.

Renforth, P., Pogge von Strandmann, P.A.E., Henderson, G.M., 2015. The dissolution of olivine added to soil: implications for enhanced weathering. Appl. Geochem. 61, 109–118. https://doi.org/10.1016/j.apgeochem.2015.05.016.

Retallack, G.J., 2005. Pedogenic carbonate proxies for amount and seasonality of precipitation in paleosols. Geology 33. https://doi.org/10.1130/g21263.1.

Rinder, T., Hagke, C.V., 2021. The influence of particle size on the potential of enhanced basalt weathering for carbon dioxide removal - insights from a regional assessment. J. Clean. Prod. 315, 128178 https://doi.org/10.1016/j.jclepro.2021.128178.

Rogelj, J., den Elzen, M., Hohne, N., Fransen, T., Fekete, H., Winkler, H., Schaeffer, R., Sha, F., Riahi, K., Meinshausen, M., 2016. Paris agreement climate proposals need a boost to keep warming well below 2 °C. Nature 534, 631–639. https://doi.org/10.1038/nature18307.

Rudmin, M., Banerjee, S., Makarov, B., Mazurov, A., Ruban, A., Oskina, Y., Tolkachev, O., Buyakov, A., Shaldybin, M., 2019. An investigation of plant growth by the addition of glauconitic fertilizer. Appl. Clay Sci. 180 https://doi.org/10.1016/j.clay.2019.105178.

SAMR, SAC, 2020. GB/T 6730.81-2020: Iron ores—determination of multiple trace elements—inductively coupled plasma mass spectrometric method. State Administration for Market Regulation and Standardization Administration of the People's Republic of China. https://openstd.samr.gov.cn/bzgk/gb/newGbInfo?hcno=751E06D0759FCE5BE668BBF4A027C216.

Shan, Y., Liu, Z., Guan, D., 2016. CO_2 emissions from China's lime industry. Appl. Energ. 166, 245–252. https://doi.org/10.1016/j.apenergy.2015.04.091.

Shi, Y., Baumann, F., Ma, Y., Song, C., Kuhn, P., Scholten, T., He, J.S., 2012. Organic and inorganic carbon in the topsoil of the Mongolian and Tibetan grasslands: pattern, control and implications. Biogeosciences 9, 2287–2299. https://doi.org/10.5194/bg-9-2287-2012.

Sochan, A., Bieganowski, A., Ryżak, M., Dobrowolski, R., Bartmiński, P., 2012. Comparison of soil texture determined by two dispersion units of Mastersizer 2000. Int. Agrophys. 26, 99–102. https://doi.org/10.2478/v10247-012-0015-9.

Solinas, S., Tiloca, M.T., Deligios, P.A., Cossu, M., Ledda, L., 2021. Carbon footprints and social carbon cost assessments in a perennial energy crop system: a comparison of fertilizer management practices in a Mediterranean area. Agric. Syst. 186, 102989 https://doi.org/10.1016/j.agsy.2020.102989.

Song, X.D., Yang, F., Wu, H.Y., Zhang, J., Li, D.C., Liu, F., Zhao, Y.G., Yang, J.L., Ju, B., Cai, C.F., Huang, B., Long, H.Y., Lu, Y., Sui, Y.Y., Wang, Q.B., Wu, K.N., Zhang, F.R., Zhang, M.K., Shi, Z., Ma, W.Z., Xin, G., Qi, Z.P., Chang, Q.R., Ci, E., Yuan, D.G., Zhang, Y.Z., Bai, J.P., Chen, J.Y., Chen, J., Chen, Y.J., Dong, Y.Z., Han, C.L., Li, L., Liu, L.M., Pan, J.J., Song, F.P., Sun, F.J., Wang, D.F., Wang, T.W., Wei, X.H., Wu, H. Q., Zhao, X., Zhou, Q., Zhang, G.L., 2022. Significant loss of soil inorganic carbon at the continental scale. Natl. Sci. Rev. 9 https://doi.org/10.1093/nsr/nwab120 nwab120.

de Souza, M.E.P., Cardoso, I.M., de Carvalho, A.M.X., Lopes, A.P., Jucksch, I., Janssen, A., 2018. Rock powder can improve vermicompost chemical properties and plant nutrition: an on farm experiment. Commun. Soil Sci. Plant Anal. 49, 1–12. https://doi.org/10.1080/00103624.2017.1418372.

Strefler, J., Amann, T., Bauer, N., Kriegler, E., Hartmann, J., 2018. Potential and costs of carbon dioxide removal by enhanced weathering of rocks. Environ. Res. Lett. 13 https://doi.org/10.1088/1748-9326/aaa9c4.

Sun, X., Liu, Q., Tang, T., Chen, X., Luo, X., 2019. Silicon fertilizer application promotes phytolith accumulation in rice plants. Front. Plant Sci. 10, 425. https://doi.org/10.3389/fpls.2019.00425.

Sun, Z., Liu, K., Liu, M., 2011. Analysis of basalt glass by electron probe micro analyzer. Rock and Mineral Analysis 30, 446–450. https://doi.org/10.15898/j.cnki.11-2131/td.2011.04.008.

Swoboda, P., Döring, T.F., Hamer, M., 2021. Remineralizing soils? The agricultural usage of silicate rock powders: a review. Sci. Total Environ. 807, 150976 https://doi.org/10.1016/j.scitotenv.2021.150976.

Tao, J., Raza, S., Zhao, M., Cui, J., Wang, P., Sui, Y., Zamanian, K., Kuzyakov, Y., Xu, M., Chen, Z., Zhou, J., 2022. Vulnerability and driving factors of soil inorganic carbon stocks in Chinese croplands. Sci. Total Environ. 825, 154087 https://doi.org/10.1016/j.scitotenv.2022.154087.

Wang, C., Li, W., Yang, Z., Chen, Y., Shao, W., Ji, J., 2015. An invisible soil acidification: critical role of soil carbonate and its impact on heavy metal bioavailability. Sci. Rep. 5, 12735. https://doi.org/10.1038/srep12735.

Xiao, L., Zhao, R., Zhang, X., 2020. Crop cleaner production improvement potential under conservation agriculture in China: a meta-analysis. J. Clean. Prod. 269, 122262 https://doi.org/10.1016/j.jclepro.2020.122262.

Yin, S., Gong, Z., Gu, L., Deng, Y., Niu, Y., 2022. Driving forces of the efficiency of forest carbon sequestration production: spatial panel data from the national forest inventory in China. J. Clean. Prod. 330 https://doi.org/10.1016/j.jclepro.2021.129776.

Zamanian, K., Pustovoytov, K., Kuzyakov, Y., 2016. Pedogenic carbonates: forms and formation processes. Earth-Sci. Rev. 157, 1–17. https://doi.org/10.1016/j.earscirev.2016.03.003.

Zamanian, K., Zarebanadkouki, M., Kuzyakov, Y., 2018. Nitrogen fertilization raises CO_2 efflux from inorganic carbon: a global assessment. Glob. Chang. Biol. 24, 2810–2817. https://doi.org/10.1111/gcb.14148.

Zeng, S., Liu, Z., Groves, C., 2022. Large-scale CO_2 removal by enhanced carbonate weathering from changes in land-use practices. Earth-Sci. Rev. 225, 103915 https://doi.org/10.1016/j.earscirev.2021.103915.

Zhang, S., Bai, X., Zhao, C., Tan, Q., Luo, G., Wang, J., Li, Q., Wu, L., Chen, F., Li, C., Deng, Y., Yang, Y., Xi, H., 2021. Global CO_2 consumption by silicate rock chemical weathering: its past and future. Earth's. Future 9, e2020EF001938. https://doi.org/10.1029/2020ef001938.

Zhao, Q.Y., Xu, S.J., Zhang, W.S., Zhang, Z., Yao, Z., Chen, X.P., Zou, C.Q., 2020. Identifying key drivers for geospatial variation of grain micronutrient concentrations in major maize production regions of China. Environ. Pollut. 266, 115114 https://doi.org/10.1016/j.envpol.2020.115114.

Zuo, W., Gu, B., Zou, X., Peng, K., Shan, Y., Yi, S., Shan, Y., Gu, C., Bai, Y., 2023. Soil organic carbon sequestration in croplands can make remarkable contributions to China's carbon neutrality. J. Clean. Prod. 382 https://doi.org/10.1016/j.jclepro.2022.135268.